Tampere University

Sanni Nousiainen

(A)SYMMETRIC ROUGHNESS OF DRIVEN ELASTIC INTERFACES IN RANDOM MEDIA

Bachelor of Science Thesis
Faculty of Engineering and Natural Sciences
Examiner: Prof. Lasse Laurson
April 2023

ABSTRACT

Sanni Nousiainen: (A)Symmetric roughness of driven elastic interfaces in random media
Bachelor of Science Thesis
Tampere University
Bachelor's Programme in Engineering and Natural Sciences
April 2023

Elastic interfaces in random media, such as domain walls in ferromagnetic thin films, have intrigued researchers worldwide for decades. The dynamics of elastic interfaces with local elasticity at zero temperature is defined by three significant forces: local elastic force, quenched noise and external driving force. The combined effect of these forces is visible on the height profile of the interface and account for the rough morphology of it. The external driving force causes the depinning transition, which is a second-order non-equilibrium phase transition between pinned and moving phases of the interface. The transition takes place at the depinning threshold, where the interface starts to continuously propagate. Individual interface elements can momentarily proceed in avalanches due to external force below the depinning threshold as well, yet mainly the interface is pinned.

At the depinning threshold, the height distribution describing the roughness of the interface has been discovered to be negatively skewed. Inspired from the discovery, this thesis examines the skewness of the distribution as the external force is increased from zero to near the depinning threshold. A numerical simulation of an elastic interface is introduced, and the results are gathered by saving an interface configuration at regular intervals as the external force is increased with a fixed rate. This is repeated 10 times with different disorder fields representing unique systems.

The results of this thesis show that as the external force is zero, the skewness of the height distribution is also approximately zero. When the external force is increased, the symmetry of the height profile starts to break due to occasional avalanches and the skewness increases as well. Eventually, the skewness starts to abate as the asymmetry of the height profile decreases, since majority of the interface elements have propagated. Near the depinning threshold the skewness is negative due to individual interface elements lagging behind the rest of the interface, which is consistent with the results of the previous research.

Keywords: elastic interface, depinning transition, roughness, asymmetry, numerical simulation

TIIVISTELMÄ

Sanni Nousiainen: Satunnaispotentiaalissa ajetun elastisen rajapinnan karheuden (epä)symmetria
Kandidaatintyö
Tampereen yliopisto
Teknis-luonnontieteellinen tutkinto-ohjelma
Huhtikuu 2023

Elastiset rajapinnat, kuten magneettisten alkeisalueiden väliset rajapinnat ferromagneettisissa ohutkalvoissa, ovat kiehtoneet tutkijoita maailmanlaajuisesti vuosikymmenten ajan. Tässä työssä tutkittavien elastisten rajapintojen dynamiikkaan lämpötilassa $T = 0$ vaikuttaa kolme merkittävää voimaa: lyhyen kantaman elastinen voima, ajasta riippumaton satunnaisvoima sekä ulkoinen ajava voima. Yksittäisten rajapinnan osien korkeus määräytyy näiden voimien yhteisvaikutuksesta, ja tuloksena muodostuu rajapinnan karhea korkeusprofiili. Rajapintaan kohdistuva ulkoinen voima aiheuttaa depinning-faasitransition, joka on jatkuva epätasapainotransitio rajapinnan liikkuvan ja jumissa olevan osan välillä. Transitio tapahtuu ulkoisen voiman saavuttaessa kriittisen arvonsa depinning-kynnyksellä, jolloin rajapinta lähtee jatkuvaan liikkeeseen. Yksittäisiä rajapinnan osien vyörymiä eteenpäin ulkoisen voiman vaikutuksesta voi tapahtua depinning-kynnyksen alapuolellakin, mutta pääosin rajapinta on tällöin jumissa.

Rajapinnan karheutta kuvaavan korkeusjakauman on havaittu olevan negatiivisesti vino lähellä depinning-kynnystä. Tästä innoittuneena tämän kandidaatintyön aiheena onkin tutkia vinouden käyttäytymistä, kun ulkoista voimaa kasvatetaan nollasta lähelle kriittistä voimaa. Rajapintaa mallinnetaan numeerisesti, ja vinouden laskemista varten tallennetaan konfiguraatio rajapinnasta tasaisin välein voimaa kasvatettaessa vakionopeudella. Tämä toistetaan 10 kertaa erilaisilla satunnaisvoimakentillä, jotka kuvaavat yksilöllisiä rajapintasysteemejä.

Tämän työn tulokset osoittavat korkeusjakauman vinouden olevan suunnilleen 0, kun rajapintaan ei kohdistu ulkoista voimaa. Kun ulkoista voimaa kasvatetaan, rajapinnan symmetria alkaa rikkoutumaan hetkellisten rajapinnan osien vyörymien vuoksi, jolloin korkeusjakauman vinous kasvaa. Kun yhä useampi rajapinnan osa on vyörynyt eteenpäin, rajapinnan epäsymmetria vähenee ja korkeusjakauman vinous pienenee. Lähellä depinning-kynnystä vinous on negatiivista, koska enää yksittäisiä rajapinnan osia on jumissa ja näin ollen jäljessä muusta rajapinnasta. Negatiivinen vinous depinning-kynnyksen läheisyydessä on yhtäpitävä aiemman tutkimuksen tuloksen kanssa.

Avainsanat: elastinen rajapinta, depinning-faasitransitio, karheus, epäsymmetria, numeerinen mallinnus

Tämän julkaisun alkuperäisyys on tarkastettu Turnitin OriginalityCheck -ohjelmalla.

PREFACE

This bachelor's thesis was made in collaboration with the Computational Physics Laboratory of Tampere University in the spring of 2023. First and foremost, I would like to thank Lasse Laurson for providing such an interesting topic and guiding me throughout the whole process. I am also thankful for my friends and family for their moral support.

Tampere, 29th April 2023

Sanni Nousiainen

CONTENTS

1. INTRODUCTION

Elastic interfaces in random media and the critical phenomena of them have been widely researched for decades. Elastic interfaces are essential in numerous systems ranging from ferromagnetic thin films [1] to earthquakes [2]. The dynamics of the interface is determined by three crucial forces: quenched noise originating from the medium, elastic force due to interactions between interface elements and external driving force [3].

The external driving force impacting the interface causes depinning transition between pinned and moving interface elements [3]. At $T = 0$, if the external force is below the depinning threshold, the interface elements are pinned, yet individual momentary avalanches may occur. As the critical force exceeds the threshold, the interface starts to continuously propagate with a finite velocity. In addition to external force, the movement of the interface is affected by quenched noise and elastic force as well. The combined effect of these three forces creates roughness on the height profile of the interface, leading to asymmetry between interface elements as some of the interface segments are proceeding while others remain pinned. The asymmetric roughness was researched by Toivonen et al. [4] with the conclusion that the height distribution of the interface is negatively skewed at the depinning threshold.

This discovery raises the question of whether the height distribution is skewed below the depinning threshold as well. Therefore, this thesis examines the dependence between the skewness of the height distribution and external driving force. Whereas previously the skewness was researched particularly at the depinning threshold, the skewness is now examined for various values of external force ranging from zero to near the critical force at the depinning threshold.

Chapter 2 introduces the physical background behind elastic interfaces and considers physical realizations of them. Numerical methods used in this thesis to describe elastic interfaces are presented in chapter 3. Chapter 3 also introduces the theory behind the topic of the research, i.e. the skewness of the height distribution. The results of the study are presented in chapter 4 and lastly, the conclusions are covered in chapter 5.

2. PHYSICAL BACKGROUND

This chapter introduces physical background of driven elastic interfaces in random media as well as some physical realizations of them. The depinning transition, which has a significant impact on defining the dynamics of an elastic interface, is also presented in this chapter.

2.1 Modeling an elastic interface

The dynamics of elastic interfaces with local elasticity can be described by the quenched Edwards-Wilkinson (qEW) equation

$$\frac{\partial h(x,t)}{\partial t} = \nabla^2 h(x,t) + \eta(x,h) + F_{ext}, \tag{2.1}$$

where $h(x,t)$ is the height variable describing an interface element, $\nabla^2 h(x,t)$ expresses the elastic force impacting an interface element, $\eta(x,h)$ is the quenched noise and F_{ext} is the external force impacting the interface [3].

The elastic force tends to keep all the interface elements on the same level, minimizing the interface energy. This thesis covers a relatively simple model of an interface and therefore the elastic force affecting an interface element is considered local. In this case, the nature of the force is determined by the neighborhood of the interface element rather than considering the impact of all the other elements. There are also systems that require considering the influence of long-range elastic interactions in order to get a full description of the interface dynamics. In such systems, the significance of the influence reduces as the distance increases [5].

The quenched noise $\eta(x,h)$ affecting the interface originates from the randomness of the medium [6]. While the elastic force attempts to level the interface, the quenched noise acts to add roughness to it. In this model, the disorder is short-range correlated, yet on a larger scale the disorder can be considered uncorrelated for both x and h. Therefore, the disorder is assumed to be normally distributed due to the central limit theorem, which states that a sum over a large amount of uncorrelated samples forms a normal distribution

[7].

Depending on the external force impacting the surface, the elastic interface has three notable states: the equilibrium ($F_{ext} = 0$), the depinning ($F_{ext} = F_c$) and the fast-flow ($F_{ext} >> F_c$), where F_c is the critical force of the depinning transition [8]. This thesis is focused on the region between the equilibrium and the depinning threshold at $T = 0$.

These three states can be described by various critical exponents. The roughness of an elastic interface, i.e. the fluctuation of the height variable $h(x, t)$, is usually described by a roughness exponent ζ, which can be determined to each state: ζ_{eq}, ζ_{dep} and ζ_{ff} [8]. The roughness exponent characterises the dependence of the interface width W on the system size L by

$$W^2(L) \sim L^{2\zeta}. \tag{2.2}$$

However, it has recently been acknowledged [4] that at the depinning threshold, a single roughness exponent ζ_{dep} is not enough to describe the rough morphology of elastic interfaces. This is due to the external force causing symmetry breaking between height values below and above the average height. This leads to different scaling properties for different segments of the interface. Therefore, for a more detailed description, a range of local exponents need to be considered as well. [4]

2.2 Depinning transition

The depinning transition is a second-order non-equilibrium phase transition between pinned and moving phases of the interface. The transition takes place at the depinning threshold, where the external force reaches its critical value F_c and pinned interface elements begin to continuously proceed. At the depinning threshold ($F_{ext} = F_c$) the velocity of the interface is still zero, but when the external force exceeds the critical force, the interface starts to continuously propagate with a finite velocity $v(F_{ext})$ [3]. The propagation velocity is proportional to the difference between the external driving force and the critical force to some power by

$$v(F_{ext}) \sim (F_{ext} - F_c)^{\beta}, \tag{2.3}$$

where β is the velocity exponent [3][6]. This applies when $T = 0$. If $T > 0$, the phase transition exhibits thermal rounding leading to non-zero propagation velocity below the critical force as well. Finite temperature therefore creates a new state for the interface between equilibrium and depinning called the creep regime. [8] This behaviour is illustrated in Fig. 2.1 [9].

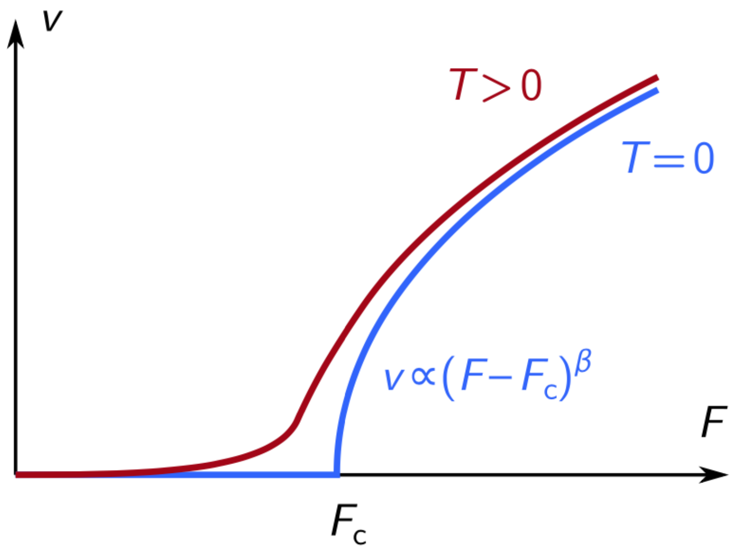

Figure 2.1. *The propagation velocity of an interface driven by an external force. Figure reprinted from [9].*

As seen in the figure, when the external force is below the critical force but differs from zero ($0 < F_{ext} < F_c$) at $T = 0$, the interface elements are pinned and $v(F_{ext}) = 0$. If slowly increased, the external force can cause the interface elements to momentarily proceed by avalanches, but eventually they become pinned again and the interface does not propagate continuously. Approaching the critical force F_c from below, the size of the avalanches in lateral direction ξ_x depends on the difference between the external force and the critical force by

$$\xi_x \sim |F_{ext} - F_c|^{-\nu_x}, \tag{2.4}$$

where ν_x is a critical exponent. The size of avalanches can also be determined in height direction ξ_h, and similarly the dependence can be written as

$$\xi_h \sim |F_{ext} - F_c|^{-\nu_h}. \tag{2.5}$$

These two approaches are proportional to the interface width by

$$\xi_h \sim W \sim (\xi_x)^\zeta, \tag{2.6}$$

where the roughness exponent ζ can be written as $\zeta = \frac{\nu_h}{\nu_x}$. [3] At $F_{ext} \gtrsim F_c$ as the interface starts to proceed continuously, the avalanche length ξ_h diverges.

2.3 Physical realizations of elastic interfaces

Different elastic interfaces can be found in various physical systems. Some physical realizations are contact lines in wetting [10], propagation of cracks in heterogeneous solid materials [11] and domain walls in ferromagnetic materials [1], for example.

A suitable example for this thesis is domain walls in ferromagnetic thin films, in which the domain walls can be approximated to be one-dimensional [1]. The elastic interface emerges between two differently polarized domains and is affected by the elastic force, quenched noise and external force stated in Eq. (2.1).

The elastic force attempts to find a state where the total energy, practically the length of the domain wall, is minimized, which in ideal situation would be the state where all the elements of the domain wall have the same height. However, the quenched noise caused by disorder in the ferromagnetic thin film can create fluctuation to the height profile of the domain wall as there are more energetically advantageous options available compared to the ideal situation. The disorder can be due to the crystal structure, impurities or crystallographic defects, such as dislocations in the thin film [12].

With ferromagnetic thin films the external force in question is an external magnetic field [1]. The external magnetic field amplifies the domain that is parallel to it at the expense of the other, causing the domain wall to move. The direction of movement depends on the orientations of the domains and the external magnetic field.

The domain wall structure can be observed by numerous imaging methods, such as spin-polarized low energy electron microscopy (SPLEEM). An illustration generated by Chen et al. [13] is presented in Fig. 2.2. The figure is a part of research in out-of-plane chiral domain wall spin-structures in ultrathin in-plane magnets, and exhibits a compound SPLEEM image of 5.2 ML Fe/15 ML Ni/W(110) bilayer system (a sketch of structure included in the figure) as well as a pixel-by-pixel magnetization vector map of it. The colour wheel included in the image represents the direction of the domain magnetization (red — [00–1], cyan — [001], green/yellow — [1–10], purple — [–110]) [13].

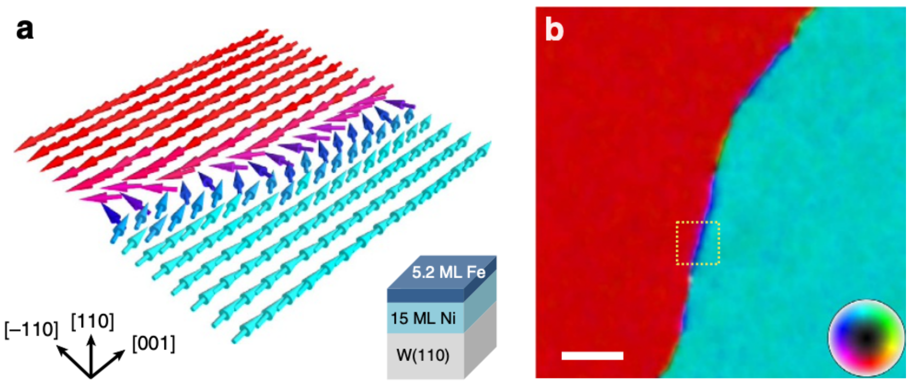

Figure 2.2. ***a)*** *Pixel-by-pixel magnetization vector map of* $350 \times 350nm$ *region of 5.2 ML Fe/15 ML Ni/W(110) system.* ***b)*** *A compound SPLEEM image of 5.2 ML Fe/15 ML Ni/W(110) system, scale bar* $500nm$*. Figure reprinted from [13].*

As Fig. 2.2 indicates, the behaviour of a driven domain wall has been simulated in various researches. Another research conducted by Xiong et al. [14] simulates a domain wall affected by an external magnetic field at zero temperature, and their illustrations are presented in Fig. 2.3. This simulation is based on the Landau-Lifshitz-Gilbert equation, which describes the magnetization dynamics in ferromagnetic materials [15]. This model is slightly more advanced compared to the qEW equation used in this thesis, it can for example describe the orientations of the magnetic domains whereas the qEW equation cannot [14]. However, both models simulate the same phenomenon and therefore the illustrations are suitable for this thesis, too.

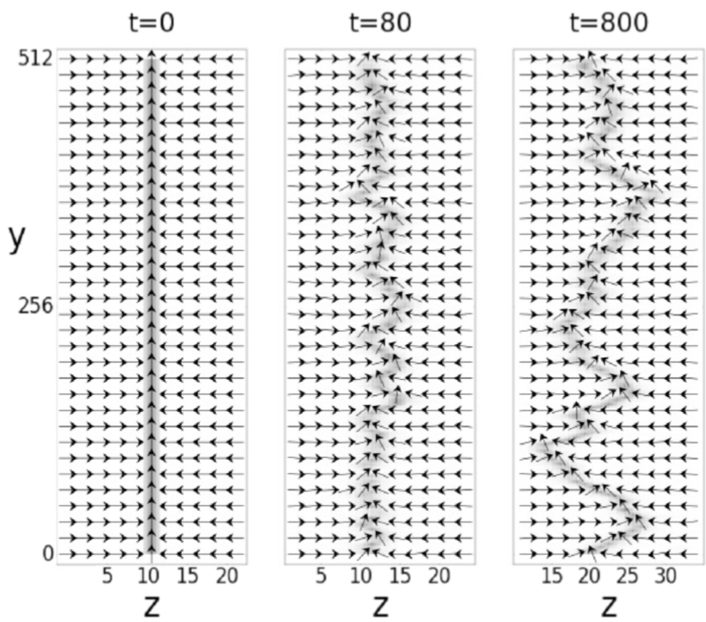

Figure 2.3. *Time evolution of domain wall affected by an external magnetic field* $H = 0.0583$*. Figure reprinted from [14].*

In this figure, y corresponds to the lateral coordinate x, z corresponds to the height coordinate $h(x)$ and the system size $L = 512$. The external magnetic field is set to go along the positive direction of the z-axis. The figure illustrates how the external driving field causes the domain wall to propagate to the positive direction of the z-axis over time. The direction of propagation is now a result of parallel magnetic field and domain, both oriented along the positive z-axis. The figure also demonstrates how the propagation of the interface is notably rough due to the disorder in the material.

3. NUMERICAL APPROACH

This chapter presents numerical methods describing elastic interfaces and takes a closer look at the height distribution of an elastic interface, which is a focal subject in this thesis.

3.1 Numerical methods

The growth equation for elastic interfaces presented in Eq. (2.1) assumes both the height variable $h(x,t)$ and the lateral coordinate x to be continuously differentiable. However, for numerical simulation the lateral coordinate needs to be discrete, which is implemented by discretizing the continuous height profile $h(x)$. The height profile is expressed with discrete segments h_i and the Laplace-operator is therefore replaced with its discrete version [16]:

$$\frac{\partial h_i(t)}{\partial t} = h_{i+1}(t) + h_{i-1}(t) - 2h_i(t) + \eta(i, h_i) + F_{ext}. \quad (3.1)$$

The time-evolution of the configuration of an elastic interface can be formed by numerically integrating this equation. In the code used for this thesis, provided by the Computational Physics Laboratory of Tampere University, the time-evolution of the configuration is determined by using the Euler method. Therefore, for an individual interface element the change of height profile h_i over time dt is calculated by

$$h_i(t + dt) = h_i(t) + F_i(h_i, t)dt, \quad (3.2)$$

where $F_i(h_i, t)$ is the total force impacting the interface element, i.e. the right side of Eq. (3.1).

In this simulation, the quenched noise acting on the interface is determined by setting normally distributed random numbers in a regular grid with unit spacing and using spline interpolation to create a continuous disorder field. The external force is increased starting from zero with a fixed rate, and the program stops approximately at $F_{ext} \approx F_c$. While the program is running, a configuration of the interface is saved at certain values of the external force. In order to get more extensive data, the program is run multiple times with different seed values in the random number generator representing unique disorder fields, and the results are then combined for each value of external force.

An example of a configuration created with the program is presented in Fig. 3.1. The data for this configuration is collected from a single run, since the configurations with different seed values are unrelated and illustrate separate interfaces.

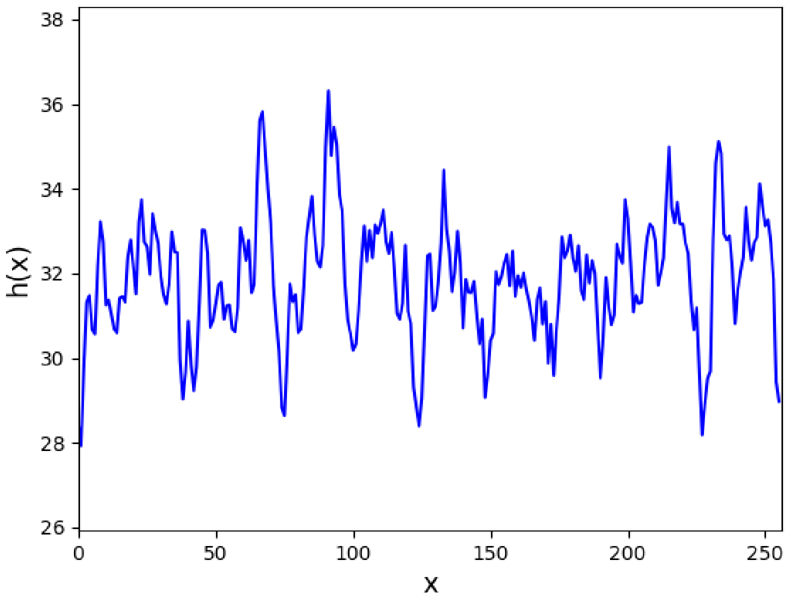

Figure 3.1. *A configuration of a relaxed elastic interface with system size* $L = 256$.

The figure illustrates a relaxed elastic interface, i.e. an interface that is not affected by an external driving force. The fluctuation of the interface is therefore caused by local elastic interactions and quenched noise.

3.2 The height distribution of an elastic interface

In this thesis the main focus is on the height distribution of an elastic interface and its properties. The height distribution $P(\tilde{h})$ is calculated for a scaled local interface height variable

$$\tilde{h} \equiv \frac{h_i - \langle h \rangle}{\sigma_h}, \tag{3.3}$$

where $\langle h \rangle$ is the mean height of the interface and σ_h is the standard deviation of the $h_i - \langle h \rangle$ values.

At the depinning threshold the height distribution $P(\tilde{h})$ has been discovered to be negatively skewed [4], thus the distribution is asymmetric. The skewness of the distribution is due to the broken asymmetry between interface elements below and above $\langle h \rangle$ caused by the external driving force [4]. If there are many interface elements with a height notably below the mean interface height, which implies they have a negative value of $h_i - \langle h \rangle$, the distribution has a long negative tail and vice versa.

In this thesis, the skewness of the distribution is calculated as the Fisher-Pearson coefficient of skewness

$$\gamma = \frac{m_3}{m_2^{3/2}}, \tag{3.4}$$

where

$$m_n = \frac{1}{N} \sum_{i=1}^{N} (h_i - \langle h \rangle)^n, \tag{3.5}$$

in which N is the size of the data set [17]. The skewness is determined for the height distributions of the configurations generated by the numerical simulation introduced in section 3.1.

4. RESULTS AND ANALYSIS

For the results, the data is combined from 10 separate runs with different seed values and a fixed system size $L = 256$. The external force is increased from zero to near the critical force and a configuration of the interface is saved at regular intervals. Due to different seed values, the program does not reach the exact same force every time and therefore the data sets for the largest values of external force are more limited. With the seed values used for the results, the critical force of the depinning transition is slightly over $F_{ext} = 1.0$ for each run.

Different runs of the program represent separate systems with unique disorder fields. The depinning transition of the interface can be detected from each run. An example of time evolution of an interface configuration captured from one run is represented in Fig. 4.1.

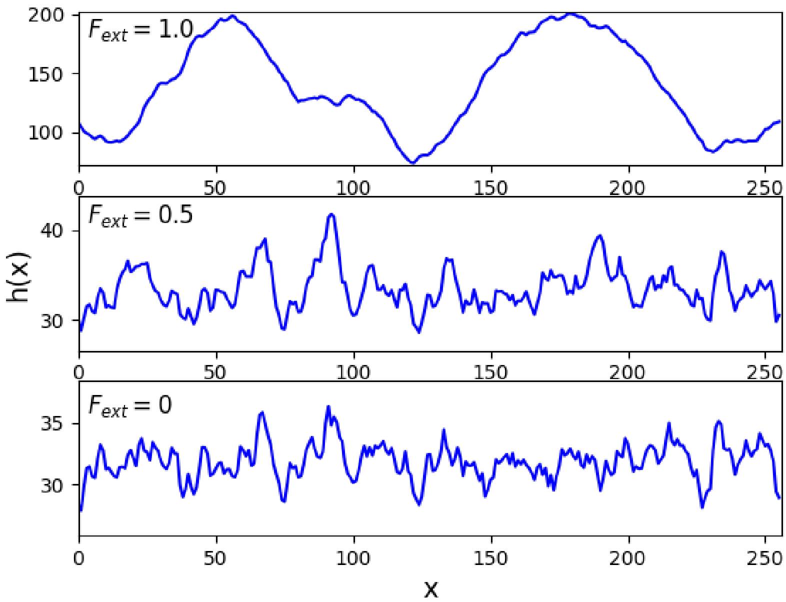

Figure 4.1. *Time evolution of the interface. The configurations are captured at $F_{ext} = 0$ (relaxed configuration), $F_{ext} = 0.5$ and $F_{ext} = 1.0$ (from bottom to top, respectively). Note unequal h-axis.*

The figure illustrates the propagation of the interface as the external force is increased. As $F_{ext} = 0$, the interface is relaxed. There is fluctuation on the height profile $h(x)$, but the values remain approximately within the interval $[27, 37]$. When the external force is increased from 0 to 0.5, the fluctuation of the interface increases as well. Individual interface elements have propagated notably further compared to the mean height of the interface. As the external force approaches the critical force, the range of $h(x)$ values is significantly larger compared to configurations with smaller driving force. At $F_{ext} = 1.0$ there is only few interface elements notably lagging behind the rest of the interface as they are still in their relaxed state, and the interface is clearly proceeding by greater avalanches in contrast to the initial configuration.

4.1 The symmetry of the height distribution

Different phases of the interface can also be observed from the height distribution $P(\tilde{h})$. The distribution is calculated for the scaled local interface height variable $\tilde{h}$ presented in Eq. (3.3). Probability densities for three data sets with different external driving force collected from a single run are illustrated in Fig. 4.2.

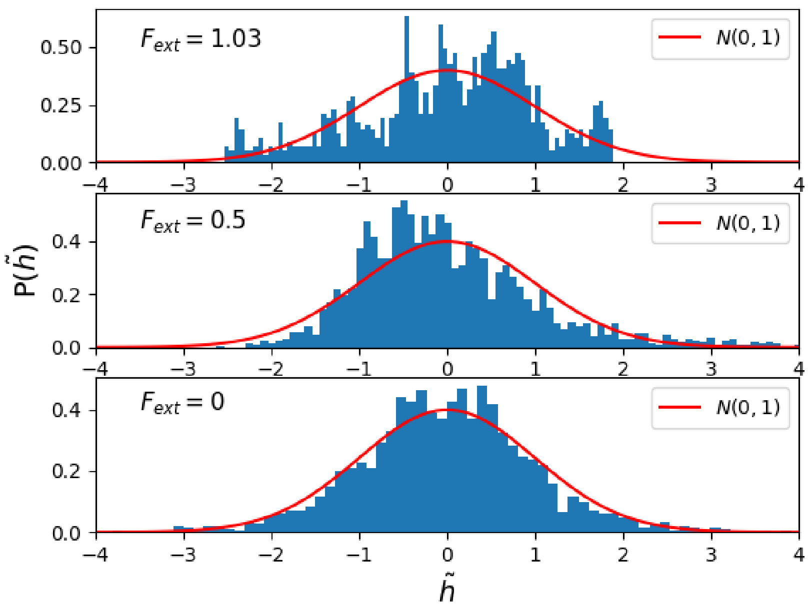

Figure 4.2. *Local interface height distributions compared to standard normal distribution $N(0,1)$. The distributions are for configurations captured at $F_{ext} = 0$, $F_{ext} = 0.5$ and $F_{ext} = 1.03$ (from bottom to top, respectively). Note unequal $P(\tilde{h})$-axis.*

As seen in the figure, the shape of the height distribution for a relaxed interface ($F_{ext} = 0$) highly resembles a probability density function of a standard normal distribution $N(0,1)$. As the external force increases, the distribution becomes more scattered and visibly skewed. At $F_{ext} = 0.5$ the distribution seems to have a long positive tail whereas at $F_{ext} = 1.03$ the negative tail appears longer.

The behaviour noted in Fig. 4.2 is examined by calculating the skewness γ for each data set. For comparison, the skewness for each data set is calculated in two ways: over the whole data set γ_{tot} and as a mean of the skewnesses from each run $\overline{\gamma}$. The error for the skewness is determined as standard error of the mean (SEM)

$$\sigma_{\overline{\gamma}} = \frac{\sigma}{\sqrt{n}}, \tag{4.1}$$

where σ is the standard deviation of the skewnesses from separate runs and n is the number of runs. The skewnesses and errors calculated for the data sets are presented in Table 4.1.

F_{ext}	γ_{tot}	$\overline{\gamma}$	Error (SEM)	Runs
0.0	0.153	0.078	0.129	10
0.1	0.294	0.193	0.121	10
0.2	0.358	0.301	0.083	10
0.3	0.693	0.493	0.106	10
0.4	0.796	0.664	0.135	10
0.5	0.972	0.795	0.089	10
0.6	1.369	0.830	0.168	10
0.7	1.051	0.775	0.072	10
0.8	1.161	0.759	0.146	10
0.9	0.523	0.170	0.132	10
1.0	0.551	0.023	0.156	10
1.01	0.388	-0.019	0.142	9
1.02	-0.166	-0.105	0.209	6
1.03	-0.447	-0.337	0.197	4

Table 4.1. *The skewnesses of the height distribution for each value of external force. The skewness is calculated over the whole data set (γ_{tot}) and as a mean of the skewnesses from each run ($\overline{\gamma}$).*

The results presented in Table 4.1 are illustrated in Fig. 4.3.

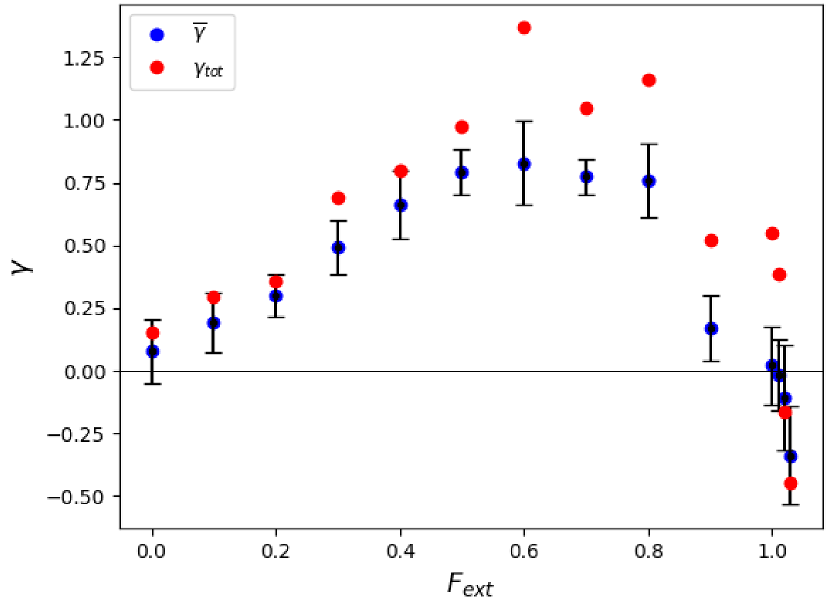

Figure 4.3. *Skewness γ as a function of external force F_{ext}. The skewness is calculated in two ways: over the whole data set (γ_{tot}) and as a mean of all separate runs ($\overline{\gamma}$). Error bars represent SEM.*

Figure 4.3 shows the dependence between the skewness of the distribution and the external driving force. When $F_{ext} = 0$, the distribution seems to be positively skewed, yet considering the error bar the skewness is approximately 0. As the external force is increased, the skewness becomes more positive up to the point of $F_{ext} \approx 0.6$. From there on, the skewness starts to decrease and near the critical force the skewness exhibits negative values. The existence of negative skewness near the depinning threshold is consistent with the results of the previous research [4].

The skewness of the height distribution, either positive or negative, can be explained by considering individual interface segments and their impact on the statistics. The length of the positive tail depends on the maximum value of the difference $h_i - \langle h \rangle$, and similar logic applies for the negative tail as well. Thus, a long positive tail results from individual interface elements located notably above the mean interface height, breaking the symmetry between values below and above the mean. This is due to some interface segments proceeding by momentary avalanches as a result of the external force. As $F_{ext} \ll F_c$, there is only a few interface elements propagating and therefore causing positive skewness to the distribution.

As the external force is increased, the interface elements proceed even further and by greater avalanches, thus there is more fluctuation on the interface. This enhances the positive skewness up to the point where majority of the interface elements have proceeded and the asymmetry starts to abate. Approaching the critical force, the skewness decreases and eventually obtains negative values. At the depinning threshold, there is individual interface segments stuck on intense pinning centers causing them to lag behind the rest of the interface. These segments have negative $h_i - \langle h \rangle$ values, which leads to a long negative tail on the distribution.

The absolute values of the skewness calculated over the whole data set are slightly greater compared to the mean values of separate runs. This is due to different mean interface heights on separate runs representing individual systems. If the skewness is calculated over the whole data set, different mean interface heights add extra variation to the height profile distorting the skewness a bit. Yet regardless of how the skewness is calculated, the results follow a similar trend.

5. CONCLUSIONS

This thesis examined the dependence between the height distribution of an elastic interface and the external force impacting it. Previous research [4] has discovered the height distribution to be negatively skewed at the depinning threshold, and hence it sparked interest towards the nature of the skewness below the depinning threshold as well.

The results show that as the external force is increased from zero to near the critical force, the skewess of the distribution increases at first. It then starts to decrease, and near the depinning threshold the skewness obtains negative values. The behaviour of the skewness can be explained by considering the propagation of individual interface elements affected by external force, local elasticity as well as quenched disorder.

For further research, the calculations could be repeated for a more extensive set of seed values. The results on this thesis are based on data of 10 different seed values, thus the reliability of the results could be improved by collecting data from a greater amount of systems with unique disorder fields. Another possible aspect for further research is to examine the skewness for different, larger system sizes as the system size used for these results is relatively small. It would also be interesting to examine whether the creep motion caused by finite temperature affects the skewness.

REFERENCES

[1] Xi, B., Luo, M.-B., Vinokur, V. M. and Hu, X. Depinning Transition of a Domain Wall in Ferromagnetic Films. *Sci. Rep. 5, 14062* (2015). DOI: 10.1038/srep14062.

[2] Jagla, E. A. and Kolton, A. B. A mechanism for spatial and temporal earthquake clustering. *J. Geophys. Res., 115, B05312* (2010). DOI: https://doi.org/10.48550/arXiv.0901.1907.

[3] Kim, J. and Choi, H. Depinning Transition of the Quenched Edwards-Wilkinson Equation. *J. Korean Phys. Soc.* 48 (2006), pp. 241–244.

[4] Toivonen, E., Molkkari, M., Räsänen, E. and Laurson, L. Asymmetric Roughness of Elastic Interfaces at the Depinning Threshold. *Phys. Rev. Lett. 129, 175701* (2022). DOI: https://doi.org/10.48550/arXiv.2209.11569.

[5] Tanguy, A., Gounelle, M. and Roux, S. From individual to collective pinning: Effect of long-range elastic interactions. *Phys. Rev. E 58* (1998). DOI: https://doi.org/10.1103/PhysRevE.58.1577.

[6] Barabási, A.-L. and Stanley, H. *Fractal Concepts in Surface Growth*. Press Syndicate of the University of Cambridge, 1995. 366 p.

[7] Fischer, H. *A History of the Central Limit Theorem. From Classical to Modern Probability Theory*. Springer, 2010.

[8] Ferrero, E., Bustingorry, S., Kolton, A. and Rosso, A. Numerical approaches on driven elastic interfaces in random media. *C. R. Physique 14* (2013), pp. 641–650. DOI: https://doi.org/10.1016/j.crhy.2013.08.002.

[9] Péterffy, G., Ispánovity, P. D., Foster, M. E., Zhou, X. and Sills, R. B. Length scales and scale-free dynamics of dislocations in dense solid solutions. *Materials Theory 4, 6* (2020). DOI: https://doi.org/10.1186/s41313-020-00023-z.

[10] Moulinet, S., Rosso, A., Krauth, W. and Rolley, E. Width distribution of contact lines on a disordered substrate. *Phys. Rev. E 69, 035103(R)* (2004). DOI: https://doi.org/10.48550/arXiv.cond-mat/0310173.

[11] Chopin, J., Bhaskar, A., Jog, A. and Ponson, L. Depinning Dynamics of Crack Fronts. *Phys. Rev. Lett. 121, 235501* (2018). DOI: 10.1103/PhysRevLett.121.235501.

[12] Zhandun, V. and Matsynin, A. The effect of the impurities on the magnetic, electronic and optical properties of Mn5Ge3. *Chin. J. Phys. 68* (2020), pp. 9–18. DOI: https://doi.org/10.1016/j.cjph.2020.06.027.

[13] Chen, G., Kang, S. P., Ophus, C., N'Diaye, A. T., Kwon, H. Y., Qiu, R. T., Won, C., Liu, K., Wu, Y. and Schmid, A. K. Out-of-plane chiral domain wall spin-structures

in ultrathin in-plane magnets. *Nat Commun 8, 15302* (2017). DOI: 10.1038/ncomms15302.

[14] Xiong, L., Zheng, B., Jin, M. H., Wang, L. and Zhou, N. J. Dynamic depinning phase transition in magnetic thin film with anisotropy. *New J. Phys. 20, 023027* (2018). DOI: 10.1088/1367-2630/aaaa27.

[15] Bertotti, G., Mayergoyz, I. D. and Serpico, C. Chapter 2 - Basic Equations for Magnetization Dynamics. *Nonlinear Magnetization Dynamics in Nanosystems*. Ed. by G. Bertotti, I. D. Mayergoyz and C. Serpico. Elsevier Series in Electromagnetism. Oxford: Elsevier, 2009, pp. 21–34.

[16] Mattos, T. G., Moreira, J. G. and Atman, A. P. F. A New Method to Study Stochastic Growth Equations: Application to the Edwards-Wilkinson Equation. *Braz. J. Phys.* 36.3A (2006). DOI: https://doi.org/10.1590/S0103-97332006000500030.

[17] *SciPy documentation. Statistical functions: skew*. URL: https://docs.scipy.org/doc/scipy/reference/generated/scipy.stats.skew.html (visited on 03/13/2023).